JOURNAL OF GEOPHYSICAL RESEARCH, VOL. 108, NO. C10, 3307, doi:10.1029/2001JC000915, 2003

Effects of wind-forcing on the dynamic spectrum in wave development: A statistical approach using a parametric model

T. Hokimoto, N. Kimura, and K. Amagai
Graduate School of Fisheries Sciences, Hokkaido University, Minato-cho, Hakodate, Japan

T. Iwamori
Field Science Center for Northern Biosphere, Hokkaido University, Minato-cho, Hakodate, Japan

M. Huzii
Research and Development Initiative, Chuo University, Shinjuku-ku, Tokyo, Japan

Received 11 April 2001; revised 30 April 2003; accepted 10 June 2003; published 2 October 2003.

[1] Previously, studies on the dynamic structure of the spectrum in the wave development process have considered only the physical mechanism of the transmission of energy from wind to wave or have considered purely mathematical methodologies. Few studies have examined the statistical mechanism of the dynamic relationship between sea surface movement, wind motion, and the time-varying spectrum of the sea surface movement. In the present paper, we investigate the statistical structure of the sea surface movement and the wind motion in developing wind waves and propose a spectral model to estimate the time-varying spectral density function. The validity of the proposed model is demonstrated through numerical experiments to evaluate the forecasting accuracy. The proposed model is used to examine the degree of the influence by wind motion, which affects the spectral density function. In the present study, we analyzed the time series record in the wave development process measured in Uchiura (Funka) Bay, Hokkaido, Japan. The basic results are summarized as follows: (1) the nonstationary statistical structure presented herein yields one of the effective classes by which to explain the dynamic mechanism between the time-varying spectral density function of sea surface movement and wind motion, and (2) in our numerical experiments the spectral model allowed effective forecasting, especially in the case of high wind speed. *INDEX TERMS:* 4263 Oceanography: General: Ocean prediction; 4203 Oceanography: General: Analytical modeling; 3210 Mathematical Geophysics: Modeling; *KEYWORDS:* wave spectrum, wave development process, forecasting, nonstationary time series model, data assimilation

Citation: Hokimoto, T., N. Kimura, K. Amagai, T. Iwamori, and M. Huzii, Effects of wind-forcing on the dynamic spectrum in wave development: A statistical approach using a parametric model, *J. Geophys. Res.*, *108*(C10), 3307, doi:10.1029/2001JC000915, 2003.

1. Introduction

[2] Numerous studies concerning the dynamic mechanism of the spectrum of the sea surface movement in the wave development process have been based on the physical structure of energy transmission from wind to wave. Such studies are based on the research of Phillips and Miles [e.g., see *Phillips*, 1957; *Miles*, 1957]. In the present paper, our primary interest is the statistical mechanism explaining how wind motion affects the spectral density function in the above mentioned situation. Here, we must consider the relationship among wind motion, sea surface movement, and the dynamic change of the spectral density function. Our goal in the present paper is to propose a statistical model to forecast the change of the time-varying spectral density function in the wave developing process. In addition, by applying the proposed model, we analyze the influence of wind forcing upon the dynamic spectrum in this process.

[3] When we estimate the spectral density function of the sea surface movement, we often use a nonparametric method such as Periodgram or the Blackman-Tukey method [e.g., see *Priestley*, 1981]. Such methods have an advantage in that they can estimate the spectral density function without assuming any time series models for the measured data. However, forecasting the change in the spectral density is necessary, the above methods of estimation are not applicable, because they contain no time-varying components. However, considering a method which is based on a parametric model allows better accuracies for both estimation and forecasting, because such a model can take physical factors (e.g., wind direction and speed) into consideration. Therefore we develop a parametric model to

0148-0227/03/2001JC000915$09.00

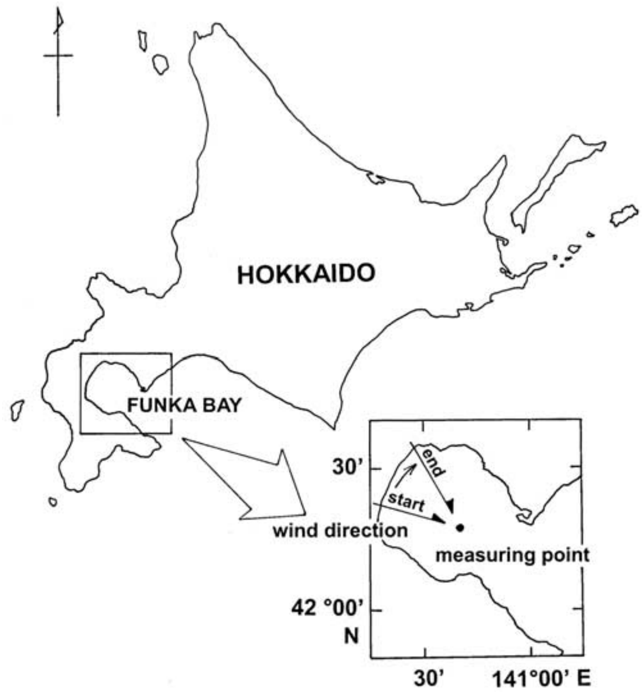

Figure 1. Map of Funka Bay and location of the sampling point.

estimate and forecast the change of the time-varying spectral density function.

[4] The present paper proceeds as follows. In the next section, we describe the physical background regarding the area of sea investigated and the method of measurement and measured data set used in the present analyses. In section 3, we propose a nonstationary spectral model to forecast the time-varying spectral density function in the wave development process. In order to examine the validity of the proposed model, we evaluate the forecasting performance via numerical experiments. The results and analyses thereof are presented in section 4. The final section presents the conclusions of the present study.

2. Physical Backgrounds of the Sea Surface Movement Generated in Funka Bay

[5] In this section, we describe the background of the area of sea investigated in the present study. In the present paper, we analyze the sea surface movement of Uchiura Bay (in the following, we use the common name, Funka Bay), Hokkaido, Japan. Figure 1 shows a map of Funka Bay. Basic research has revealed that in winter, strong seasonal wind blows frequently from the northwest. As a result, the development of wind waves is highly probable. We intend to investigate the dynamic relationship of this phenomenon. However, the dynamic relationship between wind motion and the development of waves is complicated. Our research began from the on-the-spot investigation of sea surface motion and wind motion. For the present investigation, we used the instruments of the Ushio-Maru, the training ship of Hokkaido University. We measured observations of the sea surface movement using a microwave-type wave height meter, and the changes in wind direction and speed at a height of approximately 15 meters from the sea surface were measured using an ultrasonic anemometer. The observations were recorded as analog signals which were digitized via A/D (Analog/Digital) transformation, where the time interval of sampling was 0.2 s.

[6] Figure 2 shows an example of the time series records obtained in the above mentioned measurement, when waves were developing in this bay. These records were recorded on 2 December 1999 at the sampling point 42°17′N and 140°40′E. From the top, the changes in the relative sea surface level (m), wind direction (deg.) and wind speed (m/s) are shown. Here, the origin of the sea surface level is the mean level recorded over the past 10 min. In addition, the origin of the wind direction corresponds to true north, and a positive value indicates the eastward direction. The total time interval of this measurement was 90 min and the sample size was 27000. First, let us examine the wind motion. The wind direction changes from 260 deg. to 330 deg., roughly, with a short-term oscillation of 2 $\sim$ 3 min. Using a map of the area around Hokkaido, the fetches in the above two wind directions are estimated as 17.2 miles and 19.4 miles, respectively. From the chart of wave hindcasting based on Wilson's Type IV, we determined that the difference between the energies of the waves generated under these fetches is insufficient, under the

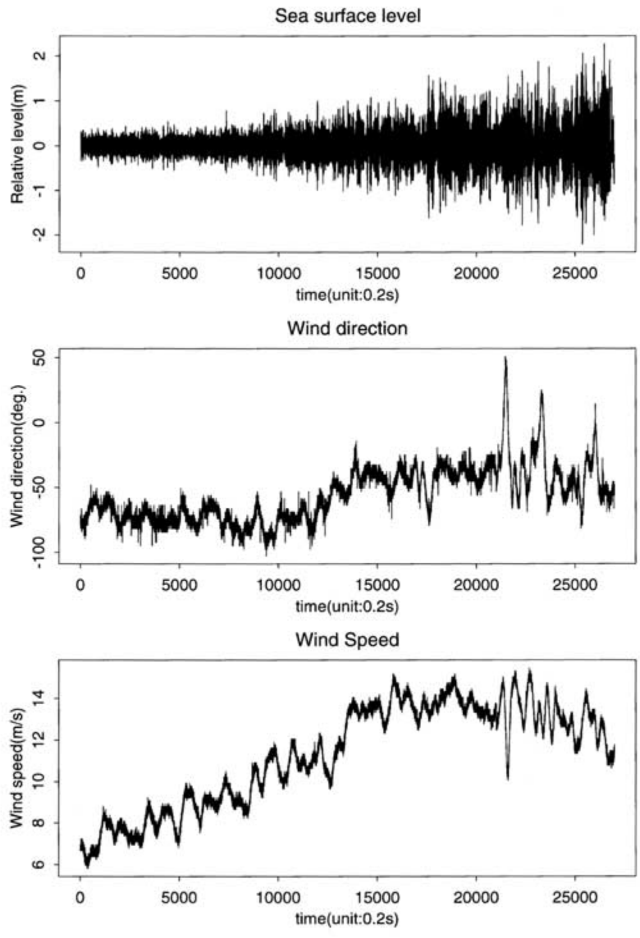

Figure 2. Time series records measured in Funka-Bay: (a) relative sea surface level (m), (b) wind direction (deg.), and (c) wind speed (m/s).

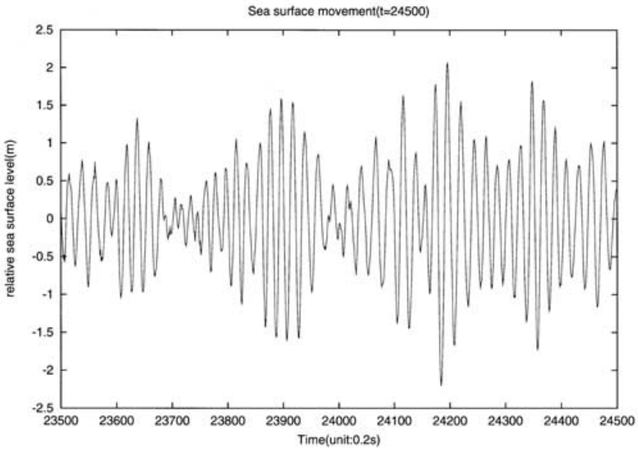

Figure 3. An example of the short-term change in the sea surface level (200 s).

condition that the wind speed is constant. Hence the records shown in Figure 2 can be regarded as an aspect of the development of the wind wave, under the situation that the fetch is almost constant. The sampling point is located at approximately the center of this bay, and the flow of wind over the fetch passes over the sampling point (see Figure 1). Furthermore, confirmation by topographical map ensures that no geographical obstacles to the flow of air by wind exist (e.g., mountains) around the fetch. Therefore we can regard these records as observations in the pure wave development process. Next, we focus on the change of relative sea surface level. Over a period of 90 min, the amplitude of the sea surface movement increases almost monotonously from 0.5 meters to 2.0 meters, which confirms that this time series data shows an aspect of the wave development process. For example, the amplitude increase approximately 1.5 meters in the range from t = 20000 to t = 25000. It this case, the amplitude increases at the rate of 0.1m/min., and after 5 min, the increment becomes 0.5 meters.

3. A Statistical Model for Forecasting the Time-Varying Spectrum in the Wave Development Process

[7] In this section, we present a statistical model by which to forecast the change of the time-varying spectrum. First, we investigate the statistical features of measured data for the sea surface movement during the wave development. Next, we present the basic concept of the spectral model proposed herein. Finally, the parameter vector of this model is considered so that wind motion is reflected in order to improve forecasting accuracy.

3.1. Statistical Structure of the Sea Surface Movement in the Developing Wind Wave and Estimation of the Spectral Density Function

[8] In the following, as a preliminary analysis to consider our spectral model, we investigate the statistical structure of the sea surface movement in the wave development process. We begin our analysis using short-term movement. Figure 3 illustrates an example of the time series record for 200 s revealing the change in relative sea surface level shown in Figure 2. Since neither the average level nor the amplitude appear to change drastically over time, we regard this time series to be stationary and estimate an autocorrelation function and a partial autocorrelation function, which are well-known methods for identifying a time series model by *Box and Jenkins'* [1970] approach. These functions are shown in Figures 4a and 4b, respectively, in which dotted lines indicate the limits of the confidence interval. As time lag increases, the former result decays slowly and the latter dumps rapidly. According to the identification procedure proposed by Box and Jenkins, these features may suggest the possibility that this time series, $\{Z_t\}$, follows a stationary autoregressive model

$$Z_t = \sum_{j=1}^{q} a_j Z_{t-j} + \delta_t \tag{1}$$

where t is a discrete time parameter, q is the order, a_j (j = 1,. . .,q) are unknown constant parameters and δ_t is a random variable which follows a white noise process with $E(\delta_t) = 0$, $E(\delta_t \delta_s) = 0 (t \neq s)$ and $E(\delta_t \delta_s) = \sigma_\delta^2 (t = s)$. In addition, the theoretical spectral density function based on equation (1) is given by [e.g., see *Brockwell and Davis*, 1991]

$$f(\lambda) = \frac{\sigma_\delta^2}{\left|1 + a_1 e^{-i2\pi\lambda} + \cdots + a_q e^{-i2q\pi\lambda}\right|^2} \tag{2}$$

where λ is the frequency. If the assumption that equation (1) is reasonable as a model of the sea surface movement is

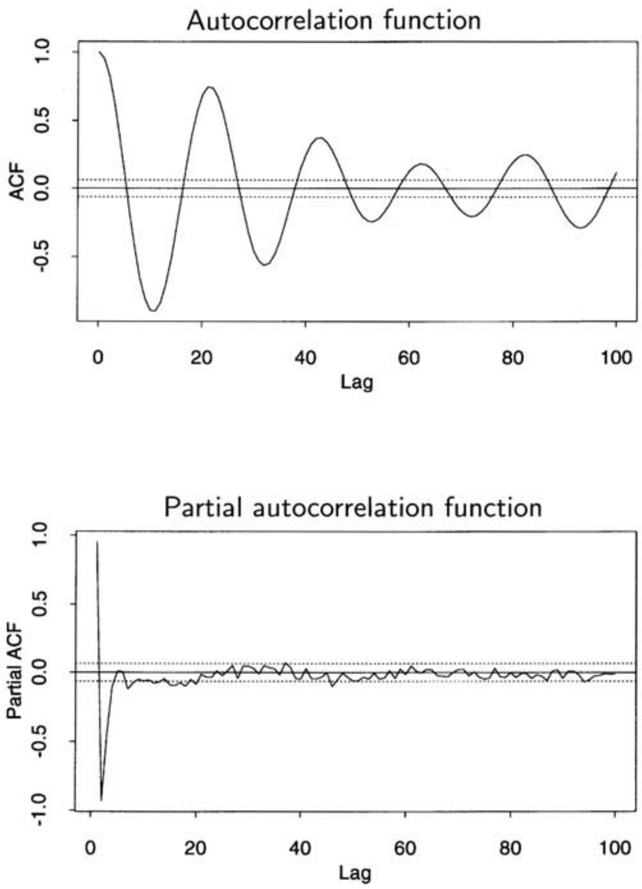

Figure 4. (a) Autocorrelation function and (b) partial autocorrelation function.

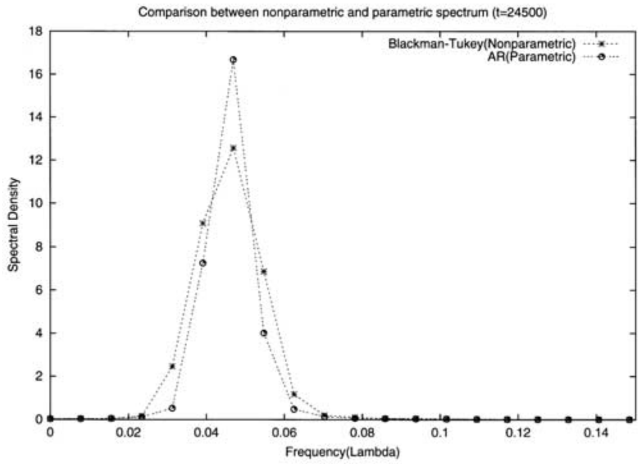

Figure 5. An overlay of $\hat{P}(\lambda)$ and $\hat{f}(\lambda)$(asterisk, $\hat{P}(\lambda)$; circle, $\hat{f}(\lambda)$).

valid, then equations (1) and (2) hold. However, since we do not know the true model of the movement, equation (2) should be examined in order to determine whether this function is reasonable as the spectral density function of the sea surface movement in this aspect. Therefore, using N samples $\{Z_1,\ldots,Z_N\}$, let us investigate the degree of agreement between the estimator of $f(\lambda)$ (denoted as $\hat{f}(\lambda)$) and the nonparametric estimator by the Blackman-Tukey method

$$\hat{P}(\lambda) = \sum_{k=-N+1}^{N-1} w(k)\hat{C}(k)e^{-i2\pi k\lambda} \tag{3}$$

where $\hat{C}(k) = 1/N\sum_{t=k+1}^{N}(Z_t - \bar{Z})(Z_{t-k} - \bar{Z})$, $\bar{Z} = 1/N\sum_{t=1}^{N} Z_t$, and $w(k)$ is a window function. For the window function $w(k)$, we use Hanning window (i.e., $w_{-1} = w_1 = 0.25$, $w_0 = 0.5$). The construction of $\hat{f}(\lambda)$ will be described in the next subsection. An example of estimations of $\hat{f}(\lambda)$ and $\hat{P}(\lambda)$ obtained using the time series data of Figure 3 is shown in Figure 5, where the asterisk indicates $\hat{P}(\lambda)$ and the circle indicates $\hat{f}(\lambda)$. These estimations appear to be in rather good agreement, which suggests that we can regard equation (2) as a basic structure of the spectrum.

[9] The above result reveals the possibility that a linear time series model (1) can be applied reasonably to explain the sea surface movement for a few minutes. In other words, this result indicates that the movement in this aspect does not exhibit strong nonlinearity. However, whether equations (1) and (2) can be applied to estimate the spectrum using the measured data for 90 min is unclear. The physical property of the wave motion in the wave development process can be expected to change over time because of the supply of energy by the wind. However, in contrast with this prediction, the parameter of equation (1) is constant. Therefore whether regarding this parameter as a constant is reasonable must be investigated. First, let us investigate the relationship between the estimated spectrum and the local time interval. Figure 6 shows the overlay of estimated values by $\hat{f}(\lambda)$ obtained at $t = 24500$ in Figure 2, under four conditions; $N = 500$ (100 s), $N = 1000$ (200 s), $N = 3000$ (600 s) and $N = 10000$ (2000 s). When N is relatively small, the estimated spectrum is slightly different from the other spectra with regard to dominant frequency and maximum value. For example, when $N = 500$, the dominant frequency is approximately 0.045 (which corresponds to a period of 4.4 s). Whereas when $N = 10000$, the dominant frequency is approximately 0.05 (4 s). In addition, the maximum value of the estimated spectrum for $N = 500$ is approximately half of that estimated for $N = 10000$. From these results, the structure of the spectrum in the wave development process is assumed to change over time, and in this sense, the statistical structure of the sea surface movement in this process has nonstationarity, even for a short time interval, such as 5 min. Next, we investigate whether the structure of spectrum changes over the time point t. Figure 7 shows an overlay of estimates by $\hat{f}(\lambda)$ obtained at different times. Figure 7a shows the change in the spectrum for every 300 s, and Figure 7b shows that for every 1000 s. Note here that the sample size N is 1000. In Figure 7a, the estimated spectrum appears to change unstably. Figure 7b indicates the following tendencies: 1) the dominant frequency becomes smaller from 0.05 (4 s) to 0.045 (4.4 s), roughly. (2) The maximum value of the estimated spectrum becomes larger(the spectrum changes more than six times). On the basis of these results, the stationarity of the sea surface movement in the wave development process is not necessarily maintainable even over a short time interval, such as 300 s.

[10] From the above observations, it is evaluated that the autoregressive model is applicable to explain the sea surface movement which generates under various conditions during the wave developing process, by taking account of time-varying structure on the parameter.

3.2. Basic Concept of the Spectral Model

[11] In this section, we present the basic concept of our spectral model. Let $\{X_t\}$ be the nonstationary process followed by the sea surface movement. On the basis of the results in the previous subsection, we assume that $\{X_t\}$ follows an autoregressive process with the pth-order time-varying coefficients

$$X_t = \sum_{j=1}^{p} \beta_{j,t}X_{t-j} + \varepsilon_t, \tag{4}$$

where $\beta_{j,t}\,(j = 1,\ldots,p)$ are unknown coefficients which change over time t, and $\{\varepsilon_t\}$ is a white noise process with

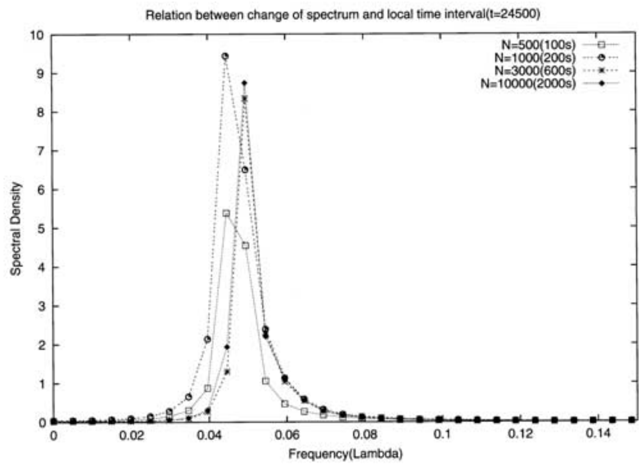

Figure 6. Relationship between $\hat{f}(\lambda)$ and the sample size (N = 500, 1000, 3000, and 10,000).

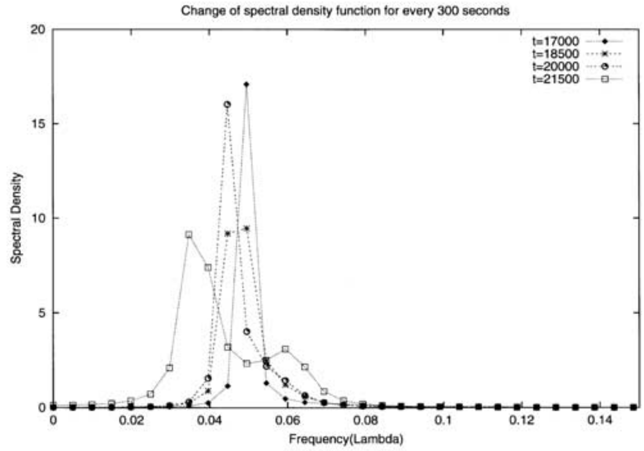

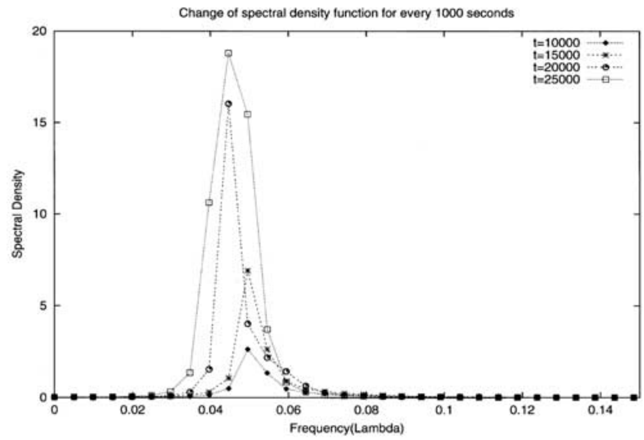

Figure 7. Change in the spectrum for each fixed time interval: (a) 300 s and (b) 1000 s.

$E(\varepsilon_t) = 0$, $E(\varepsilon_t\varepsilon_s) = 0 (t \neq s)$ and $E(\varepsilon_t\varepsilon_s) = \sigma_t^2 (t = s)$, where σ_t^2 is an unknown coefficient. The rates of change of the above coefficients are expected to be slow. Therefore these coefficients are assumed not to change significantly at any time point over a certain time interval. In other words, we regard $\beta_{j,t}$ and σ_t^2 as constant for any t in the local time interval $[t - M + 1, t]$, where M is a positive constant. Note here that the value of M is unknown, because this value depends on the degree of nonstationarity of $\{X_t\}$. In the following, we introduce another time parameter n, such that $n = k$ ($k = 1,\ldots,N$) corresponding to $t = kM$ and focus on the changes in the above parameters with respect to n. In addition, the order p is unknown and is assumed to be constant over t and n. The method used to select the values of M and p will be shown later. From equation (4), the theoretical spectral density function at the time parameter n is given by

$$f(\lambda, n) = \frac{\sigma_n^2}{\left|1 + \beta_{1,n} e^{-i2\pi\lambda} + \cdots + \beta_{p,n} e^{-i2p\pi\lambda}\right|^2} \tag{5}$$

Note here that for the estimation of parameters $(\beta_{1,n},\ldots,\beta_{p,n}, \sigma_n^2)$, we use M samples $\{X_t; t \in [(n-1)M + 1, nM]\}$. These parameters are assumed to have correlations with one another. For example, when $\beta_{1,n}$ changes significantly over n, $\beta_{2,n}$ will follow the change, although a time delay may exist. In other words, the following two possibilities exist for the change of parameter: (1) when n is fixed, $\{\beta_{1,n},\ldots,\beta_{p,n}\}$ and σ_n^2 are correlated to one another, and (2) the behavior of each parameter with respect to n has significant autocorrelation. Taking these possibilities into consideration, we explain the relationship among these parameters via the following linear equations

$$\beta_{i,n} = \sum_{j=1}^{p} a_{ij}^{(1)} \beta_{j,n-1} + \cdots + \sum_{j=1}^{p} a_{ij}^{(K)} \beta_{j,n-K} + a_{i,p+1}^{(1)} \sigma_{n-1}^2 + \cdots + a_{i,p+1}^{(K)} \sigma_{n-K}^2 + \zeta_{i,n}$$

for $i = 1,\ldots,p$, and

$$\sigma_n^2 = \sum_{j=1}^{p} a_{p+1,j}^{(1)} \beta_{j,n-1} + \cdots + \sum_{j=1}^{p} a_{p+1,j}^{(K)} \beta_{j,n-K} + a_{p+1,p+1}^{(1)} \sigma_{n-1}^2 + \cdots + a_{p+1,p+1}^{(K)} \sigma_{n-K}^2 + \zeta_{p+1,n}$$

where $\{a_{ij}^{(k)}\} (i = 1,\ldots,p + 1, j = 1,\ldots,p,\ k = 1,\ldots,K)$ are unknown coefficients, $\zeta_{i,n} (i = 1,\ldots,p + 1)$ are random variables which follow white noise processes with $E(\zeta_{i,n}) = 0$, $E(\zeta_{i,n}\zeta_{i,n}) = \sigma_{i,i}^2$ and $E(\zeta_{i,n}\zeta_{j,n}) = 0 (i \neq j)$. These relationships can be rewritten in the following form

$$\begin{pmatrix} \beta_{1,n} \\ \vdots \\ \beta_{p,n} \\ \sigma_n^2 \end{pmatrix} = \begin{pmatrix} & & \\ & a_{ij}^{(1)} & \\ & & \end{pmatrix} \begin{pmatrix} \beta_{1,n-1} \\ \vdots \\ \beta_{p,n-1} \\ \sigma_{n-1}^2 \end{pmatrix} + \cdots + \begin{pmatrix} & & \\ & a_{ij}^{(K)} & \\ & & \end{pmatrix} \begin{pmatrix} \beta_{1,n-K} \\ \vdots \\ \beta_{p,n-K} \\ \sigma_{n-K}^2 \end{pmatrix} + \begin{pmatrix} \zeta_{1,n} \\ \vdots \\ \zeta_{p,n} \\ \zeta_{p+1,n} \end{pmatrix}$$

This suggests that the state of parameters at n is expressed by a linear combination from the standpoints of frequency and time. Here, we set the parameter vector $\boldsymbol{\theta}_n = (\beta_{1,n},\ldots,\beta_{p,n}, \sigma_n^2)'$ (where the symbol $'$ indicates transposition). Then, the above relationship shows that $\boldsymbol{\theta}_n$ follows the following multivariate autoregressive model of the Kth order

$$\begin{gathered} \boldsymbol{\theta}_n = A_1 \boldsymbol{\theta}_{n-1} + A_2 \boldsymbol{\theta}_{n-2} + \cdots + A_K \boldsymbol{\theta}_{n-K} + \boldsymbol{\delta}_n \\ \boldsymbol{\delta}_n \sim WN(\mathbf{0}, \textstyle\sum) \end{gathered} \tag{6}$$

where $\{A_k = (a_{ij}^{(k)})\}$ $(k = 1,\ldots,K)$ are unknown coefficient matrices and $\boldsymbol{\delta}_n = (\zeta_{1,n},\ldots,\zeta_{p,n},\zeta_{p+1,n})'$ is the white noise vector satisfying $E(\boldsymbol{\delta}_n) = \mathbf{0}$ and $E(\boldsymbol{\delta}_n\boldsymbol{\delta}_n{}') = \mathrm{diag}(\sigma_{1,1}^2,\ldots,\sigma_{p+1,p+1}^2)$. The method used to select K will be described later.

[12] The identification of equation (6) requires estimation of the unknown coefficient matrices $A_1,\ldots,A_K$ by numerical calculation, after the value of K has been selected. When $\{\theta_l; l = 1,\ldots,n\}$ has stationarity as a process with respect to n, we can construct the Yule-Walker estimator for unknown A_k, and the solution can be computed by applying Whittle's algorithm (see Appendix A). In order to forecast future values θ_{n+l} $(l = 1,\ldots,L)$, we use a linear predictor $\tilde{\theta}_{n+l}$, which is defined by

$$\tilde{\theta}_{n+l} = \tilde{A}_1 \mathbf{z}_{n+l-1} + \tilde{A}_2 \mathbf{z}_{n+l-2} + \cdots + \tilde{A}_K \mathbf{z}_{n+l-K} \tag{7}$$

where $z_{n+l-m} = \theta_{n+l-k}$ $(l \leq k)$, $= \tilde{\theta}_{n+l-k}$ (otherwise), and $\tilde{A}_i$ is the estimator of a coefficient matrix. Using equation (7), we can obtain values for $\{\tilde{\beta}_{j,n+l}\}$ and $\tilde{\sigma}_{n+l}^2$ by the calculation of $\tilde{\theta}_{n+1},\ldots\tilde{\theta}_{n+L}$. Thus the predictor of $f(\lambda, n)$ at l steps ahead can be defined as

$$\tilde{f}(\lambda, n+l) = \frac{\tilde{\sigma}_{n+l}^2}{\left|1 + \tilde{\beta}_{1,n+l} e^{-i2\pi\lambda} + \cdots + \tilde{\beta}_{p,n+l} e^{-i2p\pi\lambda}\right|^2} \tag{8}$$

[13] Finally, we show the method used to select the unknown time interval M and the orders p and K; the selection of which affects the forecast accuracy of $\tilde{\theta}_{n+l}$, because the number of parameters to be estimated and the number of samples to be used for estimation differ depending on their values. Therefore the accuracy of the estimation of $\{A_i\}$ may be negatively affected. We select these values such that the sum of squared forecasting errors over the frequency λ, say $S = S(p(l), K(l), M(l))$, given as

$$S = \sum_{j=1}^{n-l} \int_\lambda \left(\hat{f}(\lambda, j|M(l)) - \tilde{f}(\lambda, j|p(l), K(l), M(l))\right)^2 d\lambda$$

is minimized for every forecast step l, where $p(l)$, $K(l)$ and $M(l)$ are the values of p, K and M under l, respectively, $\hat{f}(\lambda, j|M(l))$ is the nonparametric estimator equation (3) and $\tilde{f}(\lambda, j|p(l), K(l), M(l))$ is the forecasted value by equation (8) for the given values of $p(l)$, $K(l)$ and $M(l)$. Note here that the values estimated by $\hat{f}(\lambda, j|M(l))$ are obtained using the data $\{X_t; t\in[(j-1)M(l)+1, jM(l)]\}$.

3.3. Dynamic Structure of the Parameter Taking Into Account Wind Motion

[14] At this stage, our model does not have the statistical structure needed in order to explain the affect of wind motion on the spectrum. In the following, we consider the structure of the parameter vector so that the proposed model can forecast future changes in the spectral density function by taking into account the wind direction and wind speed.

[15] The behaviors of $\theta_n = (\beta_{1,n},\ldots,\beta_{p,n},\sigma_n^2)'$ are explained by the wind motion and the time histories of the parameter vector. For this purpose, we investigate the behaviors of parameters with respect to n, and the relationship between these behaviors and the wind motion. First, we look at the behaviors of estimated parameter values, obtained by piecewise estimation. Figures 8a and 8b show an example of the behavior of the estimated values of σ_n^2 and $\beta_{1,n}$ (denoted as $\hat{\sigma}_n^2$ and $\hat{\beta}_{1,n}$), respectively, when an autoregressive model of the second order is fitted to the sea surface data shown in

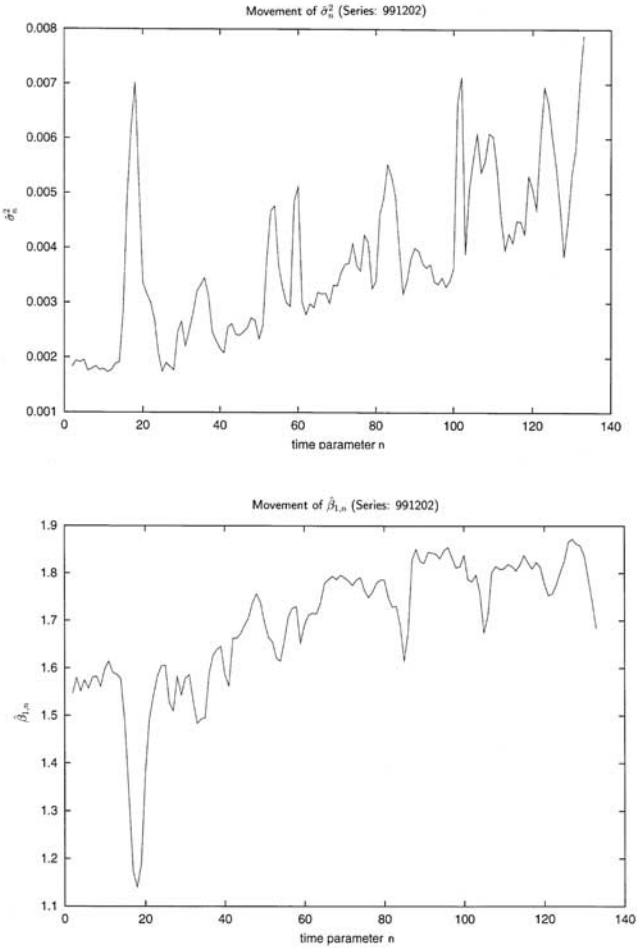

Figure 8. Behaviors of estimates: (a) $\hat{\sigma}_n^2$ and (b) $\hat{\beta}_{1,n}$.

Figure 2. In order to obtain these series, we fix the value of the local time interval M as 500 (100 s) and then fit equation (1) to the time series data obtained by updating the series after every 200 samples (40 s). In Figure 8a, $\hat{\sigma}_n^2$ has a clear tendency to increase and therefore it has a nonstationary statistical structure. In equation (5), we interpret σ_n^2 as a parameter which affects the magnitude of the spectrum. This increase is assumed to be due to the supply of energy supplied by wind forcing. Similarly, Figure 8b indicates that the behavior of $\hat{\beta}_{1,n}$ also exhibits nonstationarity with respect to n, because clear change is evident in the tendency of this behavior. $\beta_{j,n}$ affects the dominant frequency and the change is also caused by the wave development. Therefore the change in the wind direction and speed, WD_n and WS_n, should be accounted for in order to explain the behaviors of $\beta_{j,n}$ and σ_n^2.

[16] Next, we consider the method used to forecast the change in these parameters. On the basis of the above results, the model equation (6) cannot be applied directly to the change of θ_n, because these vectors exhibit nonstationarity. Thus, according to the Box-Jenkins approach, rather than focusing on θ_n, we focus on the differenced series, $\nabla \theta_n = \theta_n - \theta_{n-1}$. In order to investigate the response structure between wind motion and $\{\nabla \theta_n\}$, we use a cross-correlation function. Figures 9a and 9b show an example of cross-correlation functions between (1) $\{\nabla\hat{\beta}_{1,n}\}$ and $\{\nabla \hat{W}S_n\}$ and (2) $\{\nabla\hat{\sigma}_n^2\}$ and $\{\nabla \hat{W}D_n\}$, respectively. Note

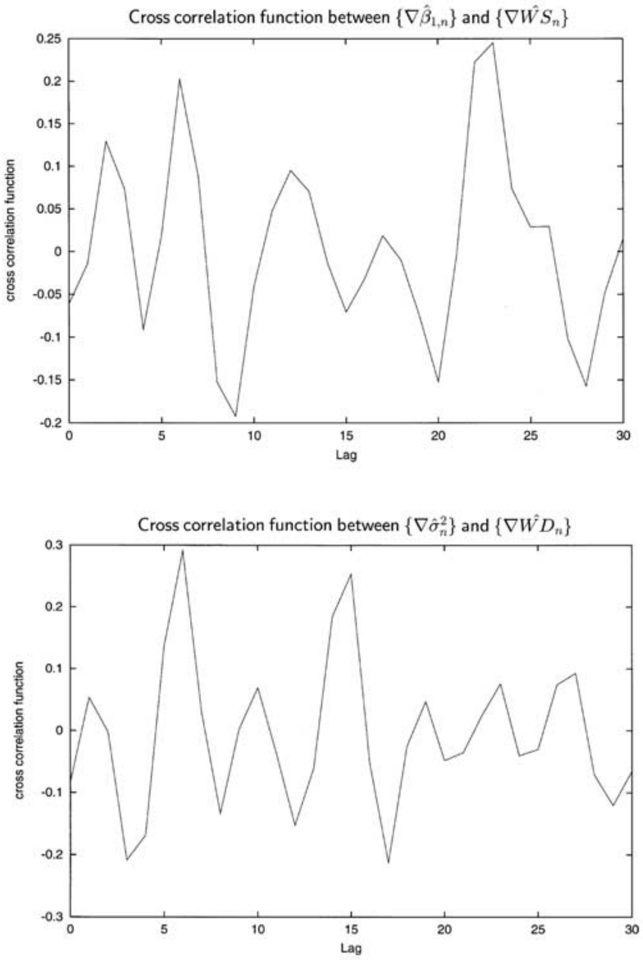

Figure 9. Cross-correlation function: (a) $\{\nabla\hat{\beta}_{1,n}\}$ and $\{\nabla\hat{W}S_n\}$ and (b) $\{\nabla\hat{\sigma}_n^2\}$ and $\{\nabla\hat{W}D_n\}$.

here that for $\{\nabla\hat{W}S_n\}$ and $\{\nabla\hat{W}D_n\}$, we used the mean value over the past 100 s. From these figures, significant correlation is found to exist between wind motion and behavior of parameters. Notably, both the wind direction and speed respond to the change in the parameter, after a delay of approximately 200 s (which corresponds to Lag = 5), which supports the hypothesis that the forecasting accuracy using the time series model equation (6) can be improved by including $\{\nabla WS_n\}$ and $\{\nabla WD_n\}$. On the basis of the above results, we define the extended state vector as

$$\boldsymbol{\theta}_n = \left(\nabla WD_n, \nabla WS_n, \left\{\nabla\beta_{j,n}; j = 1, \ldots, p\right\}, \nabla\sigma_n^2\right)' \qquad (9)$$

and assume that this vector satisfies the multivariate autoregressive model equation (6).

4. Validity of the Model From the Standpoint of Forecasting Accuracy: A Case Study

[17] Examining the validity of the proposed model requires evaluation of the forecasting accuracy of the spectral density function. From the results in subsection 3.1, we determined that the stationarity of the sea surface movement does not hold, even in the time interval of 5 min. In the following case study, we investigate the feature in forecasting the change in the spectrum over 5 min. First, we show an example of multistep forecasting of the time-varying spectral density function in the wave development process. We then evaluate the forecasting performance of this model by numerical experiments.

4.1. An Example of Forecasting the Time-Varying Spectrum

[18] First, examples of bird's eye views of the estimated spectrum and the forecasted spectrum up to 10 steps ahead (in which one step corresponds to 40 s) are shown in Figures 10a and 10b. Figure 10a shows estimates of the time-varying spectral density function obtained using measured data and Figure 10b shows the result of forecasting using the proposed model. Note that the method used to estimate the spectrum is defined in the next subsection. Both results appear to have the following tendencies: (1) the maximum value of the spectrum becomes larger with each forecasting step and in both figures generally increases. This occurs because the wave energy increases in the wave development process because of the supply of wind energy: (2) the dominant frequency gradually becomes smaller. Although, the dominant frequency of the forecasted spectrum also changes with the same tendency as that described above, the forecasted spectrum is slightly larger than that of

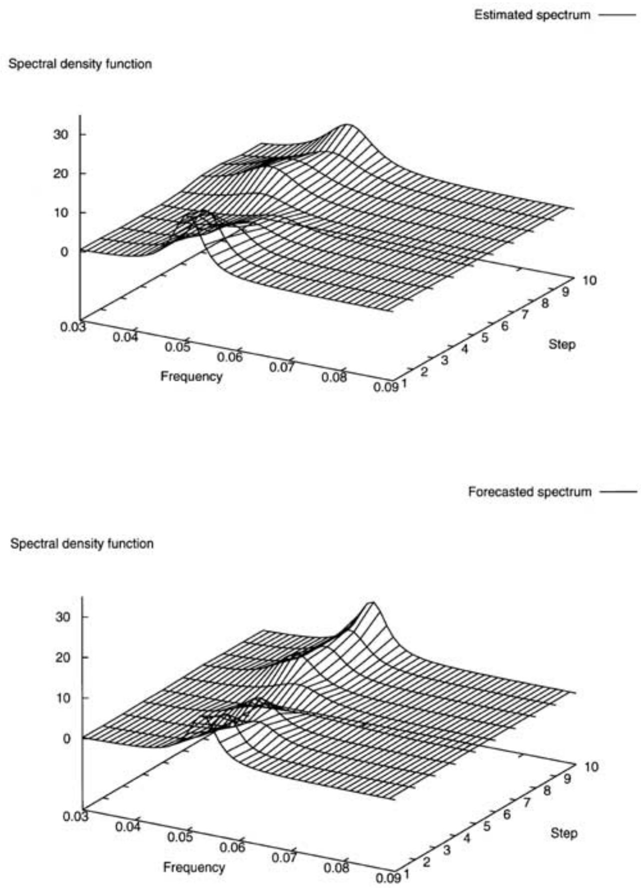

Figure 10. Bird's eye views of the change in the time-varying spectrum: (a) estimates and (b) forecasts.

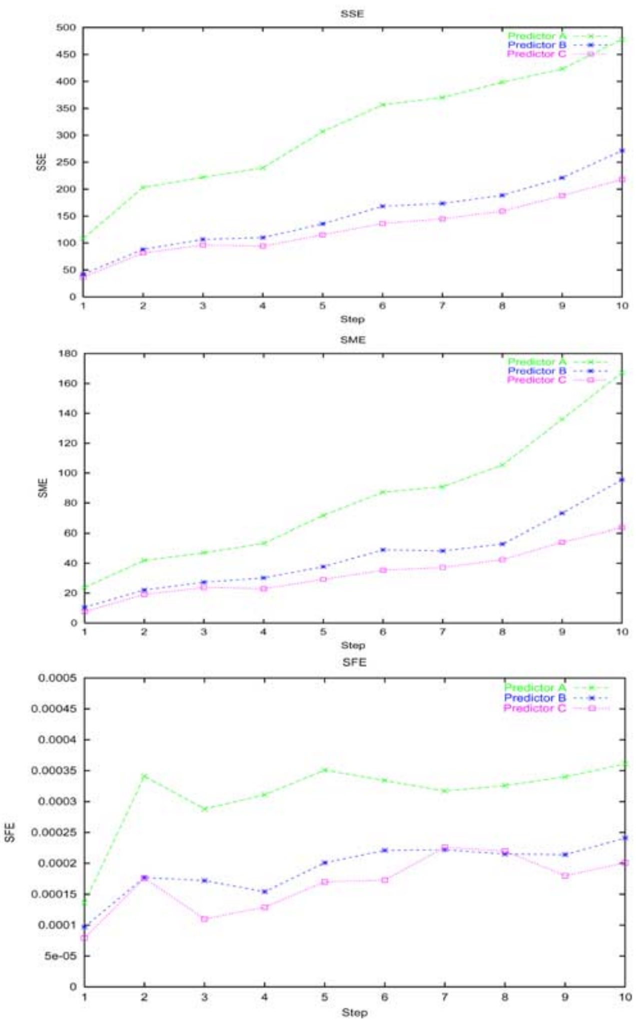

Figure 11. Performances of the three predictors: (a) $SSE(L)$, (b) $SME(L)$, and (c) $SFE(L)$.

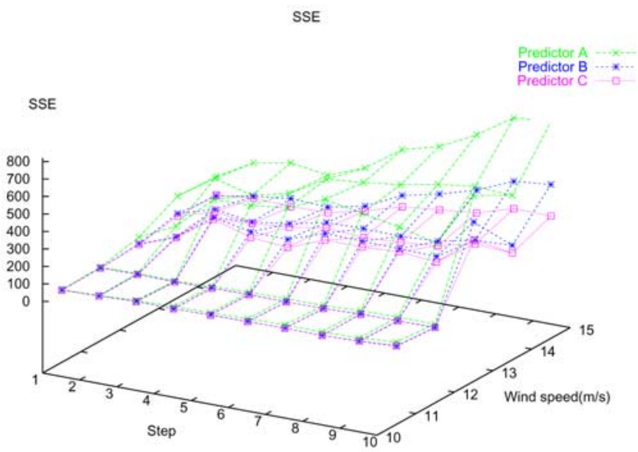

Figure 12. $SSE(L)$ given by the three predictors: green, $\tilde{f}_A(\lambda, n+l)$; blue, $\tilde{f}_B(\lambda, n+l)$; and pink, $\tilde{f}_C(\lambda, n+l)$.

the estimated spectrum. This is because the wave period becomes longer as the wave develops.

4.2. Numerical Experiment on to Examine Forecasting Accuracy

[19] When we forecast the change in the dynamic spectrum, the forecasting accuracy may change depending on the time at which forecasting starts. Therefore investigation as to whether our model can generally provide good forecasting accuracies is necessary. This analysis is performed via numerical experiments. In our experiments, we compare the forecasting performance numerically among the several methods which are expected to yield reasonable forecasts.

[20] The numerical experiment is conducted as follows. In the first stage, we randomly select a time $t = T_0$, and then obtain the forecasted spectral density function at $t = T_0 + T_s L$ ($L = 1,\ldots,10$), where T_s is a constant time interval. In the following experiments, we fix the value of T_s as 200, such that one step corresponds to 40s. For the comparison of performance, we define the following predictors:

[21] (A) Examination as to whether our assumption that the sea surface movement in the wave development process has nonstationarity is reasonable is necessary. We therefore define

$$\tilde{f}_A(\lambda, n+l) = \hat{f}_L(\lambda, n)$$

where n is the discrete time parameter introduced in subsection 3.2 and $\hat{f}_L(\lambda, n)$ is defined by the nonparametric estimator equation (3). In order to estimate $\hat{f}_L(\lambda, n)$, we use the time series data in the local time interval, $\{X_t; t \in [(n-1)M(l)+1, nM(l)]\}$. Note here that the value of $M(l)$ is optimized by minimizing S, as defined in subsection 3.2. If the statistical structure of the sea surface movement in the wave development process maintains stationarity, then this predictor gives the best performance.

[22] (B) In addition, investigation of the contribution to the effective forecasting of the spectrum due to the wind is necessary. We therefore define another predictor $\tilde{f}_B(\lambda, n+l)$ using the method presented in subsection 3.2. Here, the state vector is defined as $\boldsymbol{\theta}_n = (\beta_{1,n},\ldots,\beta_{p,n},\sigma_n^2)'$, which indicates that the behaviors of the time-varying parameters are independent of wind direction and speed. If no large differ-

Table 1. Distribution of R for Each Class of Wind Speed

Wind Speed	R
10∼11 m/s	605
11∼12 m/s	614
12∼13 m/s	1189
13∼14 m/s	2227
14∼15 m/s	865
Total	5500

Table 2. Mean Value of $SSE(L)$ Over 10 Steps for Each Class of Wind Speed

Class	10∼11 m/s	11∼12 m/s	12∼13 m/s	13∼14 m/s	14∼15 m/s
$\bar{\rho}_{AC}(1/\bar{\rho}_{AC})$	1.71(0.58)	2.18(0.46)	1.93(0.52)	2.90(0.35)	3.24(0.31)
$\bar{\rho}_{AB}(1/\bar{\rho}_{AB})$	1.70(0.59)	2.06(0.49)	1.67(0.60)	2.42(0.41)	2.38(0.42)
$\bar{\rho}_{BC}(1/\bar{\rho}_{BC})$	1.01(0.99)	1.07(0.93)	1.15(0.87)	1.20(0.84)	1.39(0.72)

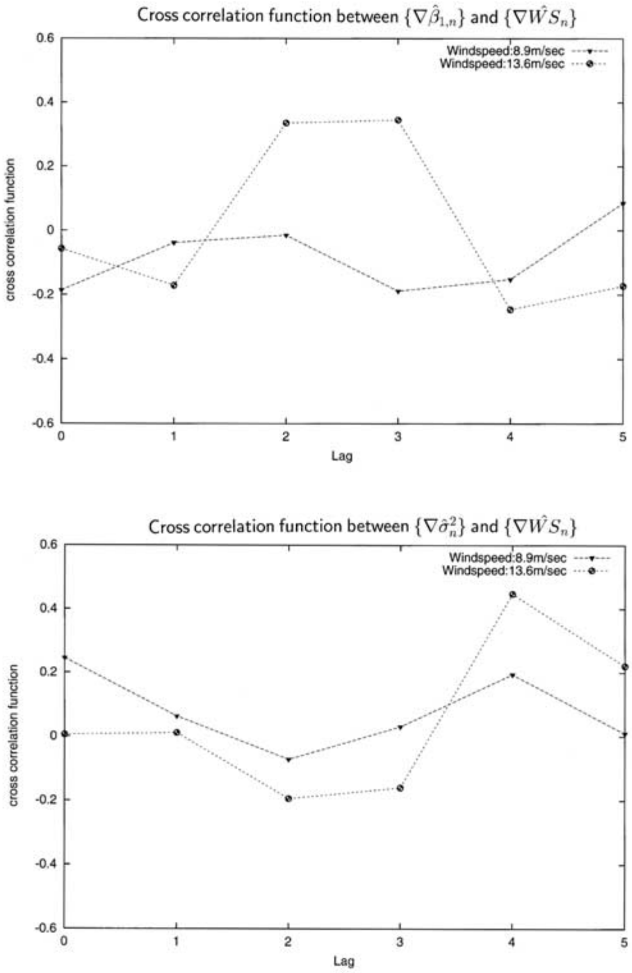

Figure 13. Cross-correlation functions for different cases of mean wind speed: (a) $\{\nabla\hat{\beta}_{1,n}\}$ and $\{\nabla\hat{W}S_n\}$ and (b) $\{\nabla\hat{\sigma}_n^2\}$ and $\{\nabla\hat{W}S_n\}$.

ences in forecasting performances exist between $\tilde{f}_B(\lambda, n+l)$ and that of the method presented in subsection 3.3, $\tilde{f}_C(\lambda, n+l)$, the change in the wind is judged to provide no contribution to the improvement of forecasting accuracy.

Table 3. Mean Value of *SME*(*L*) Over 10 Steps for Each Class of Wind Speed

Class	10∼11 m/s	11∼12 m/s	12∼13 m/s	13∼14 m/s	14∼15 m/s
$\bar{\rho}_{AC}(1/\bar{\rho}_{AC})$	2.00(0.50)	2.94(0.34)	2.20(0.46)	2.95(0.34)	3.13(0.32)
$\bar{\rho}_{AB}(1/\bar{\rho}_{AB})$	2.01(0.50)	2.01(0.50)	1.45(0.69)	2.17(0.46)	2.17(0.46)
$\bar{\rho}_{BC}(1/\bar{\rho}_{BC})$	1.01(0.99)	1.51(0.66)	1.45(0.69)	1.37(0.73)	1.47(0.68)

[23] In the second stage, we evaluate the accuracy of the forecasted spectrum. Here, several criteria must be defined in order to evaluate the forecasting performance. One criterion is the sum of squared errors:

$$SSE(L) = \frac{1}{R}\sum_{k=1}^{R}\int_{\lambda}\left[\tilde{g}^{(k)}(\lambda, T_0 + T_sL) - \hat{g}_L^{(k)}.(\lambda, T_0 + T_sL)\right]^2 d\lambda,$$
$$L = 1, \ldots, 10$$

where L is the forecast step, k is the experimental time, $\hat{g}_L^{(k)}(\lambda,\ T_0 + T_sL)$ is the estimate of the spectral density function which has been estimated locally at $t = T_0 + T_sL$ using the nonparametric estimator equation (3), and $\hat{g}^{(k)}(\lambda,\ n + l)$ is the forecasted spectrum at the same time point, using the above predictors. Note that, for the estimation of $\hat{g}_L^{(k)}(\lambda,\ T_0 + T_sL)$, we used the measured data in the local time interval $[T_0 + T_sL - T^*(L),\ T_0 + T_sL]$, where $T^*(L)$ is the unknown local time interval at step L. The value of $T^*(L)$ is determined such that the sum of squared residuals after fitting equation (1) is minimized (see Appendix B). $SSE(L)$ evaluates the degree of difference between $\hat{f}_L^{(k)}(\lambda,\ n + l)$ and $\hat{f}^{(k)}(\lambda,\ n + l)$ over the frequency. However, the maximum value and the dominant frequency of the spectrum used to minimize $SSE(l)$ may not be optimized. Therefore we define criteria by which to examine the degree of agreement for the dominant frequency and the maximum value of the spectral density function,

$$SFE(L) = \frac{1}{R}\sum_{k=1}^{R}\left[\tilde{\lambda}_{max}^{(k)}(T_0 + T_sL) - \hat{\lambda}_{L,max}^{(k)}(T_0 + T_sL)\right]^2$$

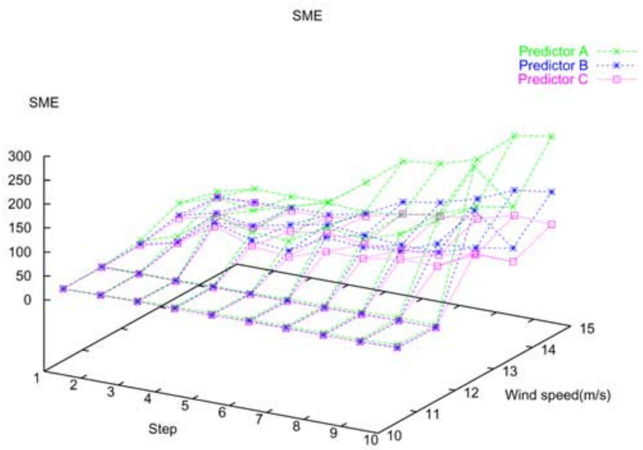

Figure 14. $SME(L)$ given by the three predictors: green, $\tilde{f}_A(\lambda, n + l)$; blue, $\tilde{f}_B(\lambda, n + l)$; and pink, $\tilde{f}_C(\lambda, n + l)$.

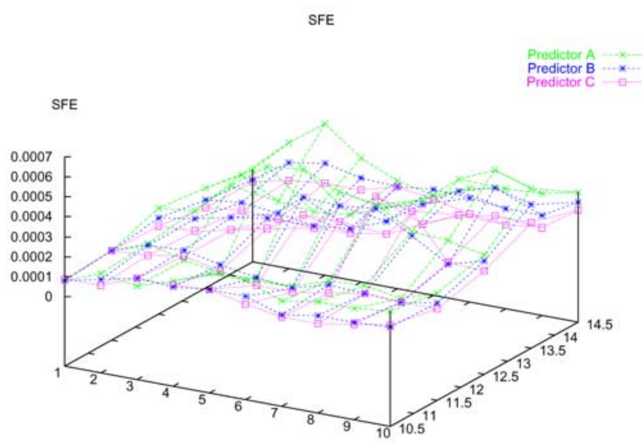

Figure 15. $SFE(L)$ given by the three predictors: green, $\tilde{f}_A(\lambda, n + l)$; blue, $\tilde{f}_B(\lambda, n + l)$; and pink, $\tilde{f}_C(\lambda, n + l)$.

Table 4. Mean Value of $SFE(L)$ Over 10 Steps for Each Class of Wind Speed

Class	10∼11 m/s	11∼12 m/s	12∼13 m/s	13∼14 m/s	14∼15 m/s
$\bar{\rho}_{AC}(1/\bar{\rho}_{AC})$	1.41(0.71)	1.26(0.79)	1.90(0.53)	2.30(0.44)	2.41(0.41)
$\bar{\rho}_{AB}(1/\bar{\rho}_{AB})$	1.33(0.75)	1.05(0.95)	1.79(0.56)	1.58(0.63)	1.48(0.68)
$\bar{\rho}_{BC}(1/\bar{\rho}_{BC})$	1.04(0.96)	1.21(0.83)	1.12(0.89)	1.45(0.69)	1.59(0.63)

and

$$SME(L) = \frac{1}{R}\sum_{k=1}^{R}\left[\max_{\lambda}\left(\tilde{g}^{(k)}(\lambda, T_0 + T_sL)\right) - \max_{\lambda}\left(\hat{g}_L^{(k)}(\lambda, T_0 + T_sL)\right)\right]^2$$

where $\tilde{\lambda}_{max}^{(k)}(T_0 + T_sL) = \arg\max_{\lambda} \tilde{g}^{(k)}(\lambda, T_0 + T_sL)$ and $\hat{\lambda}_{L,max}^{(k)}(T_0 + T_sL) = \arg\max_{\lambda} \tilde{g}_L^{(k)}(\lambda, T_0 + T_sL)$. The best predictor is expected to yield the smallest values over all forecasting steps.

4.3. Accuracy in Forecasting the Time-Varying Spectrum Using the Spectral Model

4.3.1. Total Tendencies of *SSE*(*L*), *SFE*(*L*), and *SME*(*L*)

[24] We first consider the total tendencies in the changes of $SSE(L)$, $SFE(L)$, and $SME(L)$. Figures 11a–11c show the changes in these criteria. Here, "Step" indicates the forecasting step l, and green, blue and pink lines correspond to the results obtained by $\tilde{f}_A(\lambda, n + l)$, $\tilde{f}_B(\lambda, n + l)$, and $\tilde{f}_C(\lambda, n + l)$), respectively. The number of repetitions R is 5500. In addition, we set the maximum limit in the choice of orders p and K as 8, so as not to give an excessive number of parameters for estimation.

[25] From the above mentioned figures, we find that the changes in $SSE(L)$ and $SME(L)$ have the following tendencies: (1) these predictors increase as the forecasting step increases (2) the values of these predictors as obtained by $\tilde{f}_B(\lambda, n + l)$ and $\tilde{f}_C(\lambda, n + l)$ are less than roughly 30∼60 percent of the value given by $\tilde{f}_A(\lambda, n + l)$ and (3) the value of the predictor as obtained by $\tilde{f}_C(\lambda, n + l)$ is roughly 70∼90 percent of the value given by $\tilde{f}_B(\lambda, n + l)$. In addition, $SFE(L)$ generally has the same tendency as the above two predictors, although the performance by $\tilde{f}_C(\lambda, n + l)$ changes unstably with respect to n to some extent. Therefore we assume that the statistical structure of the sea surface movement changes clearly, even over the short time interval of approximately 400 s, because the class of nonstationary statistical structure (i.e., $\tilde{f}_B(\lambda, n + l)$ and $\tilde{f}_C(\lambda, n + l)$) becomes more reasonable for forecasting the time-varying spectrum than the class based on the locally stationarity (i.e., $\tilde{f}_A(\lambda, n + l)$). In particular, in $SSE(L)$ and $SME(L)$, the difference between $\tilde{f}_A(\lambda, n + l)$ and the other two predictors tends to become larger as the forecasting step increases. This tendency can be interpreted such that the nonstationary model structure based on equation (4) gives one of the classes by which to express the change in the statistical structure of the sea surface movement. In addition, equation (7) yields one of the effective predictors for $\{\boldsymbol{\theta}_n\}$, because the performance of multistep forecasting becomes better than that of $\tilde{f}_A(\lambda, n + l)$. On the other hand, from tendency 3, we find out that the predictor taking into account the wind motion improves the performance. In Figures 11a and 11b, we also find that the difference between the performances of $\tilde{f}_B(\lambda, n + l)$ and $\tilde{f}_C(\lambda, n + l)$ becomes larger as the forecasting step increases, although the difference is not as large as in the above case. On the basis of these results, we conclude that the predictor given by equation (7) becomes more effective in multistep forecasting by including the change in wind motion. We interpret that the validity of the predictor equation (7) indicates that the dynamic structure of this predictor can explain the dynamic response structure between the wind motion and the sea surface movement to some extent.

4.3.2. General Tendency in Forecasting the Time-Varying Spectrum of the Sea Surface Movement Generated Under Various Classes of Wind Speed

[26] We now evaluate the forecasting accuracy when the above three predictors are applied to measured data of the sea surface movement generated under various classes of wind speed. In this case, the range of the distribution of wind speed is 10 m/s∼15 m/s. According to Beaufort scale, the following three classes of wind speed, 10 m/s∼11 m/s, 11 m/s∼14 m/s and 14 m/s∼15 m/s, respectively belong to fresh breeze, strong breeze and near gale, and physical properties of the waves which are generated under these wind classes are different with one another. However, since it is not necessarily guaranteed that this classification is strictly reasonable for our research sea area, in the following experiments, we define a class of wind speed for every 1 m/s increment. We grouped the numerical results of $SSE(L)$, $SFE(L)$, and $SME(L)$ as obtained in the previous experiment into five classes according to the value of wind speed just before the forecast start time. The distribution of the repetition time R for each of the above mentioned classes is shown in Table 1. For every class of wind speed, we obtained the mean value of each criteria for use as a summary statistic.

[27] First, we examine $SSE(L)$. Figure 12 shows the performances of the three predictors for each class of wind speed. In addition, as a summary statistic, the mean values of the relative ratios, $r_{AC}(L) = SSE_A(L)/SSE_C(L)$, $r_{AB}(L) = SSE_A(L)/SSE_B(L)$ and $r_{BC}(L) = SSE_B(L)/SSE_C(L)$, over 10 steps,

$$\bar{\rho}_{AC} = \frac{1}{10}\sum_{L=1}^{10} r_{AC}(L), \qquad \bar{\rho}_{AB} = \frac{1}{10}\sum_{L=1}^{10} r_{AB}(L),$$
$$\bar{\rho}_{BC} = \frac{1}{10}\sum_{L=1}^{10} r_{BC}(L)$$

and their reciprocals are shown in Table 2. In Figure 12, green, blue and pink lines correspond to the results obtained using $\tilde{f}_A(\lambda, n + l)$, $\tilde{f}_B(\lambda, n + l)$ and $\tilde{f}_C(\lambda, n + l)$, respectively. According to the results for $1/\bar{\rho}_{AC}$ and $1/\bar{\rho}_{AB}$ in Table 2, the values of $SSE(L)$ obtained by $\tilde{f}_B(\lambda, n + l)$ and $\tilde{f}_C(\lambda, n + l)$, which are based on the nonstationary structure, give roughly 30∼60 percent of that obtained by $\tilde{f}_A(\lambda, n + l)$, although the percentage varies with the class of wind speed, suggesting that the nonstationary statistical structure positively affects forecasting of the time-varying spectrum for all classes of wind speed. In addition, the result for $\bar{\rho}_{BC}$ shows that 1) in the classes of 10 m/s∼12 m/s, no significant difference in forecasting performance is found between the predictors $\tilde{f}_B(\lambda, n + l)$ and $\tilde{f}_C(\lambda, n + l)$. The values $1/\bar{\rho}_{BC}$ for these classes are 0.99 and 0.94. 2) in the classes of 12 m/s∼15 m/s, $\tilde{f}_C(\lambda, n + l)$ gives better performance than $\tilde{f}_B(\lambda, n + l)$, because $SSE(L)$ obtained by $\tilde{f}_C(\lambda, n + l)$ is roughly 70∼90 percent of that obtained by

$\tilde{f}_B(\lambda, n+l)$, and 3) the value of $1/\bar{\rho}_{BC}$ becomes smaller. Thus we find that $\tilde{f}_C(\lambda, n+l)$ becomes a more effective predictor from the standpoint of $SSE(L)$, as the wind speed increases.

[28] In order to examine why $\tilde{f}_C(\lambda, n+l)$ becomes effective as the wind speed increases, let us once more investigate the response structure between the parameter in equation (4) and wind speed. Figures 13a and 13b display the cross-correlation functions between (1) $\{\nabla\hat{\beta}_{1,n}\}$ and $\{\nabla\hat{W}S_n\}$ and (2) $\{\nabla\hat{\sigma}_n^2\}$ and $\{\nabla\hat{W}S_n\}$, respectively, for different cases of wind speed. Here, triangles indicate the estimated spectrum using the sea surface movement generated under the mean wind speed of 8.9 m/s, and circles indicate that using the movement under the mean wind speed of 13.6 m/s. In both figures, we find that the latter cross correlation takes larger values than that the former cross correlation, indicating that, as the wind speed increases, the wind motion has a stronger impact on the change in the parameters in equation (4). Therefore, as the wind speed increases, multistep forecasting of $\{\boldsymbol{\theta}_n\}$ using the predictor equation (7) becomes more effective, and as a result, $\tilde{f}_C(\lambda, n+l)$ yields better forecasting performance than $\tilde{f}_A(\lambda, n+l)$ or $\tilde{f}_B(\lambda, n+l)$.

[29] Next, we focus on $SME(L)$. Figure 14 shows the change in $SME(L)$ and Table 3 shows the results for $\bar{\rho}_{AC}$, $\bar{\rho}_{AB}$ and $\bar{\rho}_{BC}$ and their reciprocals. We can ensure that the value of $SME(L)$ obtained by $\tilde{f}_A(\lambda, n+l)$ tends to increase as the wind speed increases, which indicates that the magnitude of the spectral density function estimated using measured sea surface data is increasing, because $\tilde{f}_A(\lambda, n+l)$ is constant over any l. Basically, the result shows the same tendencies as $SSE(L)$. According to Table 3, we find that the $SME(L)$'s obtained by $\tilde{f}_B(\lambda, n+l)$ and $\tilde{f}_C(\lambda, n+l)$ are roughly 30∼70 percent of that obtained by $\tilde{f}_A(\lambda, n+l)$. Furthermore, the $SME(L)$ obtained by $\tilde{f}_C(\lambda, n+l)$ is roughly 60∼70 percent of that obtained by $\tilde{f}_B(\lambda, n+l)$, although no large differences exist among the three predictors for wind speeds of 10 m/s∼12m/s. In this case, $\bar{\rho}_{BC}$ is small even for lower wind speeds, and $1/\bar{\rho}_{BC}$ is approximately 70 percent for the classes of 11 m/s∼15 m/s. This implies that our model can provide a large positive effect to forecast maximum values of the time-varying spectrum.

[30] Finally, we investigate the effectiveness of the proposed predictors for forecasting dominant frequencies. Figure 15 shows the results for $SFE(L)$ and Table 4 shows the values of $\bar{\rho}_{AC}$, $\bar{\rho}_{AB}$ and $\bar{\rho}_{BC}$ and their reciprocals. The general tendencies of the results are basically identical to the above two criteria. These results are summarized as follows: 1) the nonstationary structure considered in our model gives better forecasting accuracy for dominating frequency than for the class of stationarity, because the values of $1/\bar{\rho}_{AC}$ and $1/\bar{\rho}_{AB}$ are distributed in the range from 40 to 95 percent. 2) $\tilde{f}_C(\lambda, n+l)$ can further improve the performance by $\tilde{f}_B(\lambda, n+l)$ up to approximately 60 percent by taking into account the change in wind, although this is not necessarily effective for classes such as 10 m/s∼11 m/s.

5. Summary and Discussion

[31] On the basis of the numerical results obtained in the previous section, let us consider the physical background on the relationship among the change of wind speed, the motion of wind wave and its nonstationary spectrum. In Table 2, for example, we may divide the values of $\bar{\rho}_{BC}(1/\bar{\rho}_{BC})$ into 3 classes; for the scaling of wind speed, we can classify 10m/s∼12m/s, 12m/s∼14m/s and 14m/s∼15m/s. Also, this classification is similar to that by Beaufaut scale, to some extent. This leads to a result that as wind wave develops, the accuracy in forecasting wave motion becomes better. It is possible to explain this result essentially from a physical standpoint. Suppose that, when wind wave develops, the kinetic energy by wind motion E, which is a function of the wind speed v_w, is completely transmitted to the potential energy of the water particles. Since E is proportional to v_w^2, the instantaneous change of E (i.e., $|dE/dv_w|$) is proportional to v_w. Hence, as v_w increases, the instantaneous change of E becomes more sensitive to the change of v_w, and as the result, the cross correlation between the change of wind speed and the behavior of wind wave becomes larger (Figures 13a and 13b illustrate this fact). Also, it suggests that as wind speed increases, the accuracies in forecasting wave motion and the change of its nonstationary spectrum can be improved by using a statistical model of autoregressive type, because the information of cross correlation between the time histories of wave motion and wind speed is used in estimating parameters of this model.

[32] Thus we can mention that the nonstationary spectral model presented here, which takes account of the structure of cross correlation between the change of wind speed and the sea surface movement, can give reasonable forecasting on the whole, and the forecasting accuracy can be improved further in the case of high wind speed.

Appendix A: Method for Estimation of the Multivariate Autoregressive Model

[33] We assume the process $\{\boldsymbol{\theta}_l;\ l = 1...,n\}$ is stationary and let $\boldsymbol{\mu}$ be the mean vector of $\boldsymbol{\theta}_l$. In equation (6), post-multiplying $\boldsymbol{\theta}'_{n-j}$ ($j = 0,...,K$) and taking the expectations yields the following $K+1$ equations

$$\Sigma = \Gamma(0) - \sum_{j=1}^{K} A_j \Gamma(-j)$$

and

$$\Gamma(i) = \sum_{j=1}^{K} A_j \Gamma(i-j), \qquad i = 1, \ldots, K$$

where $\Gamma(i)$ is the autocovariance matrix of $\boldsymbol{\theta}_n$. By replacing $\Gamma(i)$ ($i = 0,\ldots,K$) by the estimator of the autocovariance matrix, $E[(\boldsymbol{\theta}_{n+i} - \boldsymbol{\mu})(\boldsymbol{\theta}_n - \boldsymbol{\mu})']$, viz.

$$\hat{\Gamma}(i) = \begin{cases} 1/n \sum_{l=1}^{n-h} \left(\boldsymbol{\theta}_{l+i} - \bar{\boldsymbol{\theta}}_n\right)\left(\boldsymbol{\theta}_l - \bar{\boldsymbol{\theta}}_n\right)' & 0 \le h \le n-1 \\ \hat{\Gamma}'(-i) & -n+1 \le h < 0 \end{cases}$$

where $\bar{\boldsymbol{\theta}}_n = 1/n \sum_{l=1}^{n} \boldsymbol{\theta}_l$. We can obtain $A_1,\ldots,A_K$ and Σ by the solution of the above $K+1$ equations. The solution can be computed by applying Whittle's algorithm [e.g., see *Brockwell and Davis*, 1996; *Brockwell and Davis*, 1991].

Appendix B: Estimation of $\hat{g}_L(\lambda, T_0 + T_s L)$

[34] First, the local time interval $T(L)$, which we can regard $\{X_t\}$ in the time interval $[T_0 + T_s L - T(L) + 1, T_0 + T_s L]$ to be a stationary time series, must be estimated. We choose the value of it, say $T^*(L)$, such that the sum of squared residual errors of X_t when the autoregressive model equation (1) is fitted,

$$SSR(T(L)) = \frac{1}{T(L)} \sum_{t=T_0+T_sL-T(L)+1}^{T_0+T_sL} \left(X_t - \hat{X}_t\right)^2$$

is minimized with respect to $T(L)$, where $\hat{X}_t$ is the estimated model using the data over the time interval $[T_0 + T_s L - T(L) + 1, T_0 + T_s L]$. For the estimation of the model, we determined the order by Akaike Information Criterion (AIC) and estimated the parameters using the least squares method. Thus $\hat{g}_L(\lambda, T_0 + T_s L)$ is estimated by (3), using the data in $[T_0 + T_s L - T^*(L) + 1, T_0 + T_s L]$.

[35] **Acknowledgments.** The comments from two anonymous reviewers were very helpful to improve our paper and we are very grateful to their contributions. Also, we thank the captain and crew members of Ushio-Maru for supporting the observation.

References

Box, G. E. P., and G. M. Jenkins, *Time Series Analysis: Forecasting and Control*, Holden-Day, Boca Raton, Fla., 1970.

Brockwell, P. J., and R. A. Davis, *Time Series, Theory and Methods*, Springer-Verlag, New York, 1991.

Brockwell, P. J., and R. A. Davis, *Introduction to Time Series and Forecasting*, Springer-Verlag, New York, 1996.

Miles, J. W., On the generation of surface waves by share flow, *J. Fluid Mech.*, *3*, 185–204, 1957.

Phillips, O. M., On the generation of waves by turbulent wind, *J. Fluid Mech.*, *2*, 417–445, 1957.

Priestley, M. B., *Spectral Analysis and Time Series*, vol. 1, Academic, San Diego, Calif., 1981.

K. Amagai, T. Hokimoto, and N. Kimura, Graduate School of Fisheries Sciences, Hokkaido University, 3-1-1 Minato-cho, Hakodate, Hokkaido 041-8611, Japan. (hocky@fish.hokudai.ac.jp)

M. Huzii, Research and Development Initiative, Chuo University, Shinjuku-ku, Tokyo 162-8473, Japan.

T. Iwamori, Field Science Center for Northern Biosphere, Hokkaido University, 3-1-1 Minato-cho, Hakodate, Hokkaido 041-8611, Japan.